Materials Transactions, Vol. 48, No. 5 (2007) pp. 924 to 930
Special Issue on New Developments and Analysis for Fabrication of Functional Nanostructures

Ion Implantation Induced Martensite Nucleation in SUS301 Steel

Hiroshi Kinoshita, Heishichiro Takahashi, Dwi Gustiono, Norihito Sakaguchi, Tamaki Shibayama and Seiichi Watanabe

Center for Advanced Research of Energy Conversion Materials, Hokkaido University, Sapporo 060-8628, Japan

Phase transformation behaviors of the austenitic 301 stainless steel was studied under Fe^+, Ti^+ and Ar^+ ions implantation at room temperature with 100, 200 and 300 keV up to fluence of 1×10^{21} ions/m^2 and the microstructures were observed by means of transmission electron microscopy (TEM). The plane and cross-sectional observations of the implanted specimen showed that the induced-phases due to implantation from the γ matrix phase were identified as α' martensite phases with the orientation relationship of $(1\bar{1}0)_\alpha$ // $(11\bar{1})_\gamma$ and $[111]_\alpha$ // $[011]_\gamma$ close to the Kurdjumov–Sachs (K–S). The ion implantation induced phases nucleated near the surface region and the depth position of the nucleation changed depending on the ion accelerating energy and ion species. It was also found that the induced marten sites phases nucleate under the influence of the stress distribution, which is introduced due to the concentration of implanted ions, especially due to the stress gradient caused by the corresponding concentration gradient. [doi:10.2320/matertrans.48.924]

(Received November 6, 2006; Accepted February 7, 2007; Published April 25, 2007)

Keywords: *stainless steel, phase transformation, induced-martensite transformation, ion implantation, concentration gradient*

1. Introduction

Stainless steels are important structural materials for nuclear reactors, offshore plants, industry and housing. Therefore, improvement of these materials to provide higher performance is required. It is well known that ion implantation is a very useful surface modification technique to produce the higher performance and the functional gradient materials,[1,2] and that ion implantation onto austenitic stainless steel improves the tribological behavior of the surface, wear characteristics and the corrosion resistance.[3–11] These surface characteristics are often closely related to transformed martensite phase formed on the surface.

In ion implantation technique, the distribution of transformed phase depends on accelerating energy, so it is possible to produce martensite phase in surface region with nano-scale. A lot of studies on the mechanism and process of transformation due to implantation with different ion species have been conducted in several types of stainless steels by means of microstructural observation using transmission electron microscopy (TEM), glancing angle X-ray diffraction, Rutherford backscattering and Mossbauer spectroscopy.[12–30]

From these investigations it has been clarified that the phase transformation from austenite γ phase to α' martensite phases is induced by ion implantation with alloy constituent elements of steels (Fe, Cr and N), heavy ions (P, Sb and Mo etc.) and inert gas ions (H, He, Ar, Kr and Xe etc.) into austenitic stainless steel such as 316 type and 304 type stainless steels.

From transmission electron microscopic investigations so far it has been revealed that material structures are damaged due to the irradiation process of ion implantation and often lattice defects are introduced,[12,13,17,25] and the phases with various size are formed near the ion-implanted surface region.[13,19,25] The fraction and size of the induced phase increased with increasing of ion fluence but the irradiation-induced α' phase transformation is independent from the implanted ion species such as austenitic stabilizer element (Ni), ferrite stabilizer element (Cr) and inert gaseous element (Ar).[19] It has also been confirmed that the relationship between austenite γ matrix and the irradiation induced α' phase is closer to the relation of Kurdjumov–Sachs.[17,31] Furthermore, it has been indicated that martensitic transformation will be associated with the stress concentration caused by the concentration of implanted ions.[18,19,21,22] However the detailed process and mechanism related to effects of implanted ions for the phase transformation during implantation are not clarified.

In present paper the effects of implanted ions on the initiation of phase transformation in 301 stainless steel was studied by the observation of microstructures related to phase transformation under ion implantation of Fe^+, Ti^+ and Ar^+.

2. Experimental Procedures

Commercial grade austenitic 301 stainless steel disks with 3 mm in diameter were cut from the foil with 0.15 mm in thickness, and annealed at 1373 K for 0.5 hour to eliminate the remained strain. The foils for transmission electron microscopy (TEM) observation were prepared by electrolytic polishing using a twin jet technique in a solution of 95% acetic acid and 5% perchloric acid at 289 K and foils for cross-sectional observation were prepared using focused ion beam (FIB).

The Fe^+, Ti^+ and Ar^+ ions were implanted into foil specimens up to a fluence of 5×10^{20} ions/m^2 at accelerating energies of 100, 200 and 300 keV at room temperature using an 400 keV ion accelerator. The projected ranges of these ions species in austenitic 301 stainless steel were calculated by TRIM code. The microstructures were observed by transmission electron microscopes with 200 keV (JEOL JEM-2000FX and JEOL JEM-2010F).

The chemical composition of 301 stainless steel used was given in Table 1.

3. Results and Discussion

3.1 Plane observation of ion implanted specimens

Figure 1(a, b, c) shows the microstructures when the foil

Table 1 Chemical composition of 301 stainless steel (mass%).

Cr	Ni	Mn	Si	Mo	N	Cu	P	Al	C	O	S
17.46	6.19	1.6	0.48	0.18	0.17	0.16	0.025	0.003	0.021	0.0021	0.0018

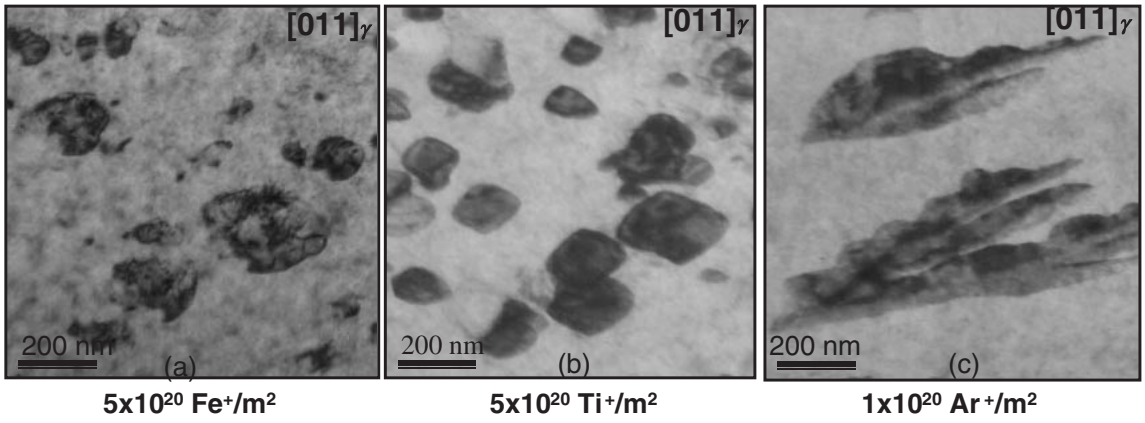

Fig. 1 Microstructures of the transformed phases after ion implantation with Fe^+, Ti^+ and Ar^+ to the fluence of (a) 5×10^{20} Fe^+/m^2, (b) 5×10^{20} Ti^+/m^2 and (c) 1×10^{20} Ar^+/m^2 at room temperature.

specimens of 301 stainless steel were implanted up to a fluence of 5×10^{20} ions/m^2 with Fe^+ and Ti^+ and to 1×10^{20} ions/m^2 with Ar^+ at room temperature. It is observed that the small phases with different shapes were formed with dispersion like precipitate, and were block-like for the Fe^+ and Ti^+ implantation, while for Ar^+ implantation the phase with the irregularly elongated shape was formed even with lower fluence of implantation comparing with other two ion species. Thus the shape of the induced phase was different depending on ion species whether the ions species are solid or gaseous. The gaseous clusters such as bubble-like state may formed in stainless steel in the case of Ar^+-ions, so that the complicated stress distribution is introduced around the clusters comparing with the case of solid ion.

In order to identify the structure of the phase induced by implantation shown in Fig. 1, the structures were analyzed from selected area diffraction pattern.

Figure 2(a, b, c) show the microstructures observed in the austenite (γ) matrix with $[011]_\gamma$ zone axis. The newly formed phases were visible in the area with damage structure such as dislocations. In these figures, the dotted circles indicate the areas where diffraction patterns were taken. From the analysis of the diffraction patterns from matrix and the induced phase, it was identified that the induced phases are transformed martensite and the orientation relation between the matrix and the induced phases were $(01\bar{1})_\alpha$ // $(\bar{1}11)_\gamma$ and $[011]_\gamma$ // $[111]_\alpha$ corresponding to Kurdjumov-Sacks orientation relation.[28–30] Thus the phase transformation takes place not with the uniformly covered surface but as the separately dispersed phase. This means that the phase transformation may initiate at localized small region.

In order to study the effect of defects evolution during implantation on martensite transformation, the defect evolution process under implantation was observed. The results were shown in Fig. 3. It is observable that a lot of defects clusters were introduced in the early stage of implantation and with increasing of Ti^+ ion dose the defects clusters were formed. The diffused pattern from the dark contrast area appeared (Fig. 3(b)) in diffraction pattern, which suggested the occurrence of transformation with further increasing of ion dose to 7.64×10^{18} Ti^+/m^2. The results suggest that defects clusters and the implanted ions are contributing to the initiation of transformation through the increasing of internal stress (internal energy).

3.2 Profiles of implanted ions and induced defects

The distribution profiles of implanted ion and defects concentration induced due to implantation depend on the ion accelerating energies and ion species. The profiles can be calculated according to TRIM code. The theoretically calculated profiles for Fe^+, Ti^+ and Ar^+ ions at 300 keV energy were given in Fig. 4(a), and Fig. 4(b) shows the profile for the energies of 100 keV, 200 keV and 300 keV Ti^+ ions. It is expected from this calculation that the peaks of implanted concentration will locate at the depth of around 100 nm, 120 nm and 150 nm for Fe^+, Ti^+, and Ar^+ at 300 keV, respectively, and the peak positions of Ti^+ ion are about 40 nm, 75 nm and 120 nm from surface at energies of 100 keV, 200 keV and 300 keV, respectively. Thus the peak of concentration appears at deeper region for the ion implantation with lighter mass, and or at higher ion energy. The profile of implanted ion concentration has been measured experimentally in previous report,[29] and it was confirmed that the profile of ion concentration obtained by calculation is coincident with the measured one by EDS.

The cross-sectional structures of transformed phases corresponding to the phase of plane observation in Fig. 1 were observed after for Fe^+, Ti^+ and Ar^+ ion implantations at 300 keV to 5×10^{20} ions/m^2 at R.T. The cross-sectional foils were prepared by FIB where W was coated on the specimen surface to protect surface from the damage due to Ga ion. Typical examples of the observed structures after implanting Fe^+, Ti^+ and Ar^+ with 300 keV accelerating voltage were shown in Fig. 5. The top surface with dark

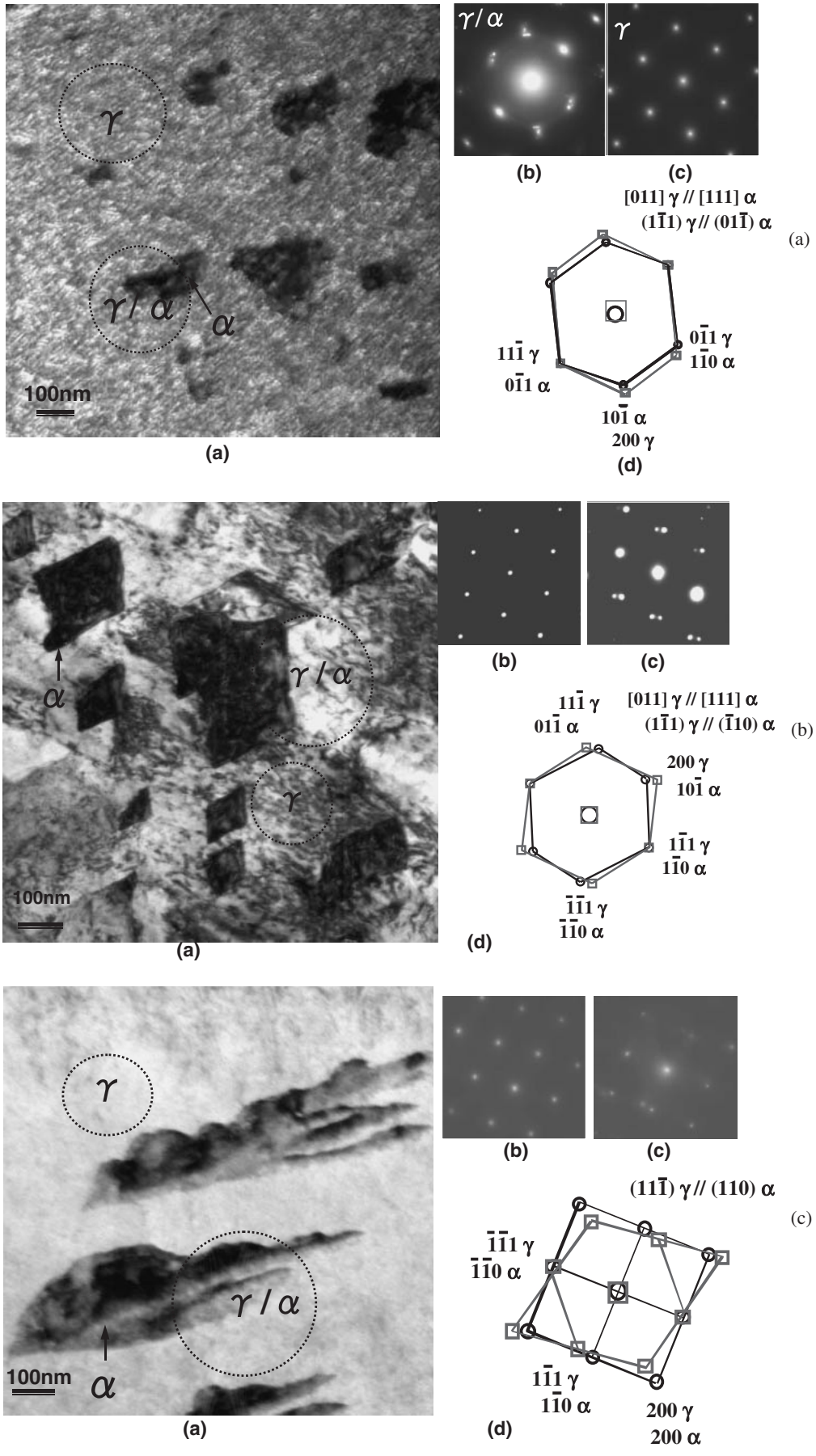

Fig. 2 Analysis of transformed phases by selected area diffraction after ion implantation with 5×10^{20} ions/m^2 at room temperature; (a) Fe^+ implantation (b) Ti^+ implantation and (c) Ar^+ implantation.

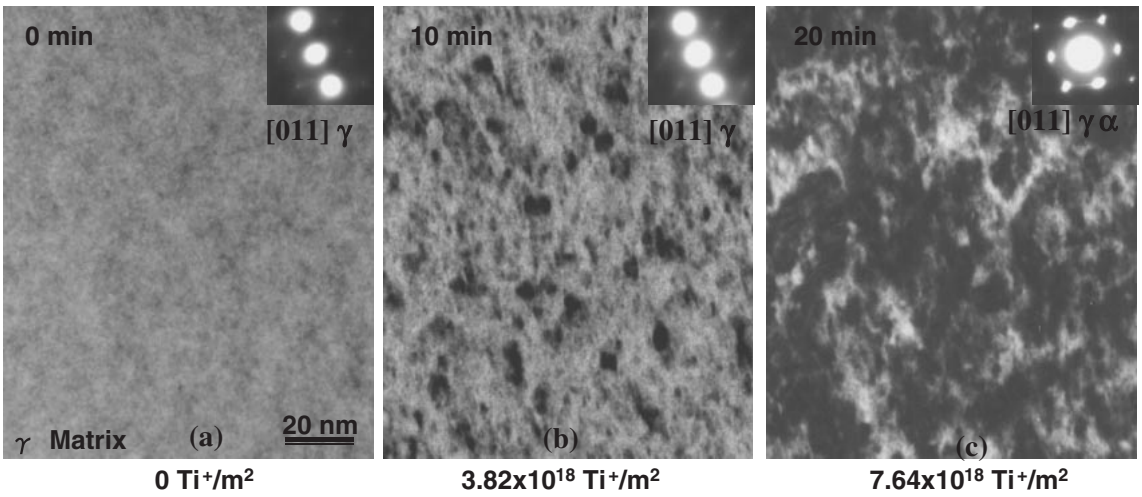

Fig. 3 Microstructural change during Ti^+ ion implantation at room temperature with near the $[011]_\gamma$ zone axis; (a) before ion implantation, (b) defect cluster formation, and (c) initiation of martensite transformation.

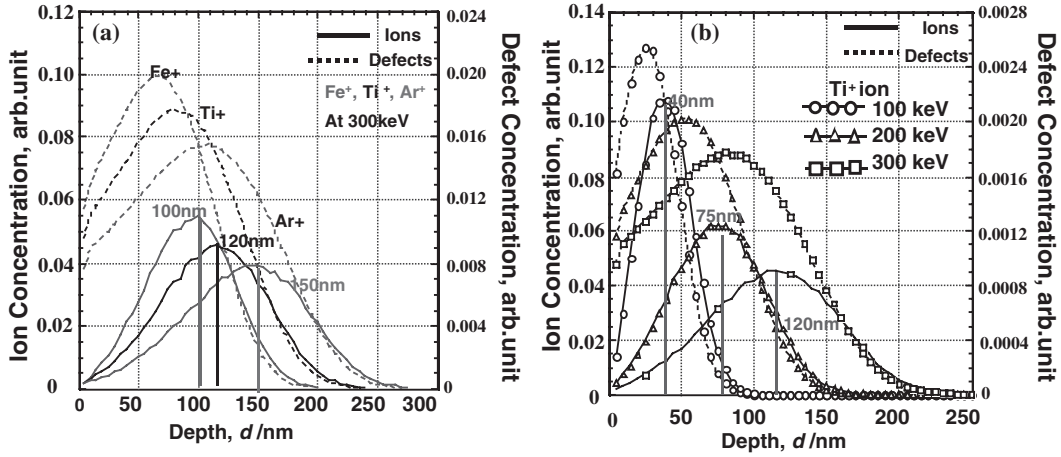

Fig. 4 Calculated profiles of concentration of implanted ions and the induced defects as a function of depth; (a) for the implantion with Fe^+, Ti^+ and Ar^+ at 300 keV, and (b) for the implantion with Ti^+ at 100 keV, 200 keV and 300 keV.

contrast corresponds to the coated W film, and the induced martensite phase as indicated by arrow was obviously observed below the W coating film.

It is obvious that the martensite phase was formed in the restricted region near surface, and furthermore the distribution of the induced phase was different depending on ion species. It is also observed that the transformation generally occurred toward surface of specimen from a given depth position rather than propagating inward. This fact suggests that martensite transformation starts at a given depth region and the transformation propagates toward surface side. When the peak positions of concentration of implanted ions and defects calculated by TRIM code in the Fig. 4 and the locations of initiation of transformation were compared, the depth positions of the induced martensite phases observed were not coincident with those calculated (see Fig. 5). This suggests that besides direct effects of the introduced defects and total amount of ion concentration, other effects may influence additionally on the initiation of martensite transformation.

3.3 Effect of implantation energy on nucleation of phase transformation

In order to study the effect of acceleration ion energy on the nucleation of phase transformation, ion implantation of Ti^+ was carried out at room temperature. The typical cross-sectional structures were shown in Fig. 6 with the calculated peak positions of ion and the defects concentration (in Fig. 3). As being seen in the figure, the depth of the calculated and the observed martensite phase positions was different, thus it is not recognized that maximum concentrations of the implanted ion and/or the introduced defects would directly associated with initiation of martensite transformation in this case as shown in Fig. 2.

3.4 Effect of implanted ion on initiation of transformation

As being shown in above results the phase transformation was induced due to the ion implantation at room temperature in the restricted region near surface but the initiation position of transformation was different from that calculated one.

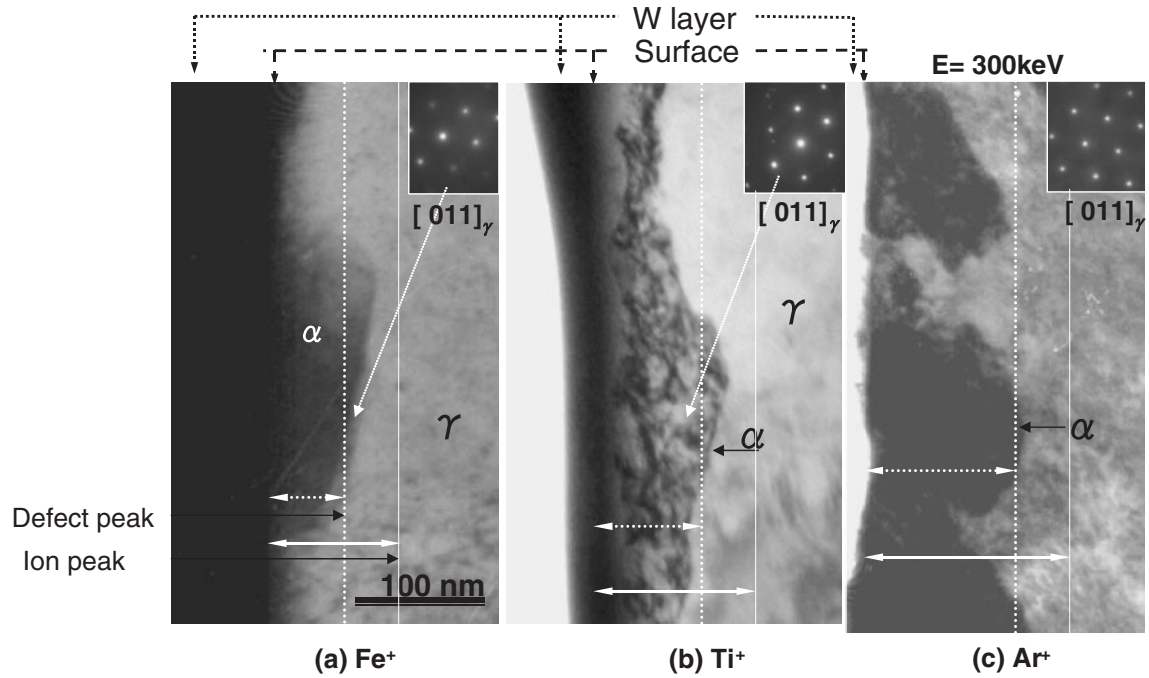

Fig. 5 Cross-sectional observation of microstructure of transformed phase after implantation with 300 keV: by (a) Fe^+, (b) Ti^+ and (c) Ar^+.

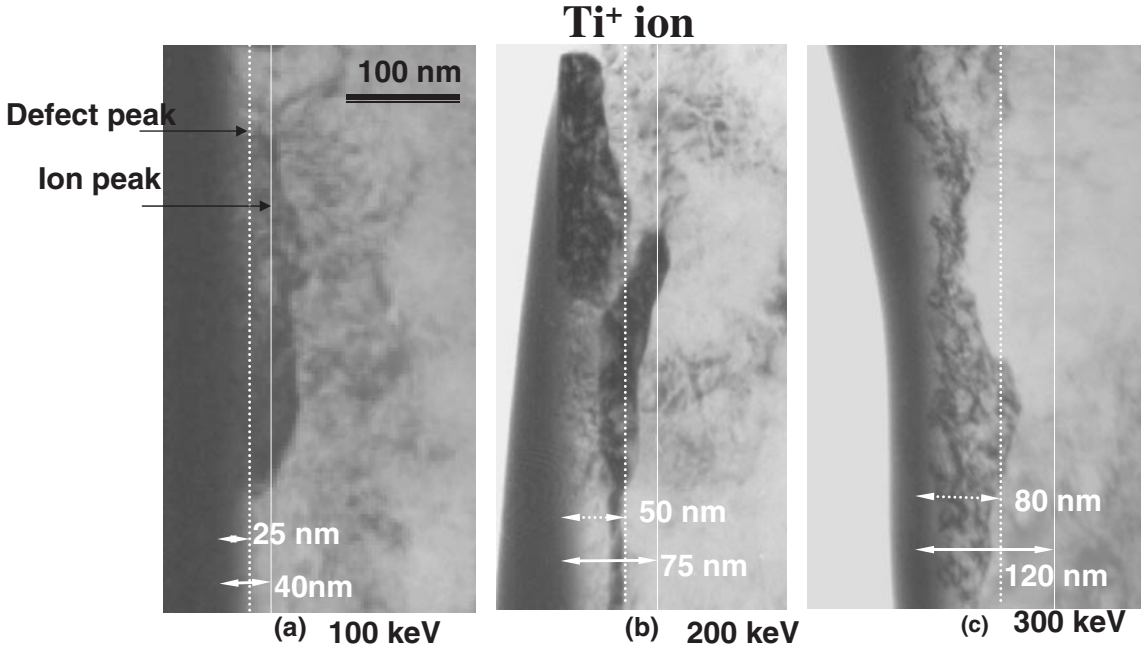

Fig. 6 Cross-sectional observation of transformed phase after Ti^+ implantation (a) at 100 keV, (b) at 200 keV and (c) at 300 keV.

Therefore, we should consider the process of the transformation under ion implantation based on mechanisms which are not directly depend on the peak concentration of ion and/or defects. Furthermore it was observed that the transformation started after a given dose of ion implantation, namely the damage defects were introduced before the phase transformation took place. Thus it is sure that defects might have a role for the phase transformation and simultaneously the implanted ion concentration might contribute it even though the total amount of the concentration do not directly affect. By considering these experimental facts, the effects of damage and the implanted ion concentration as main factors would associate with to the initiation of phase transformation. The stress distribution profiles calculated by considering the volume expansion due to the implanted ion were shown In Fig. 7(a), where the average volume change was estimated by the following relation, ε (strain) = V (ions)/(V (matrix) + V (ions), σ (compressive stress) = $\varepsilon \cdot$ K, K; bulk

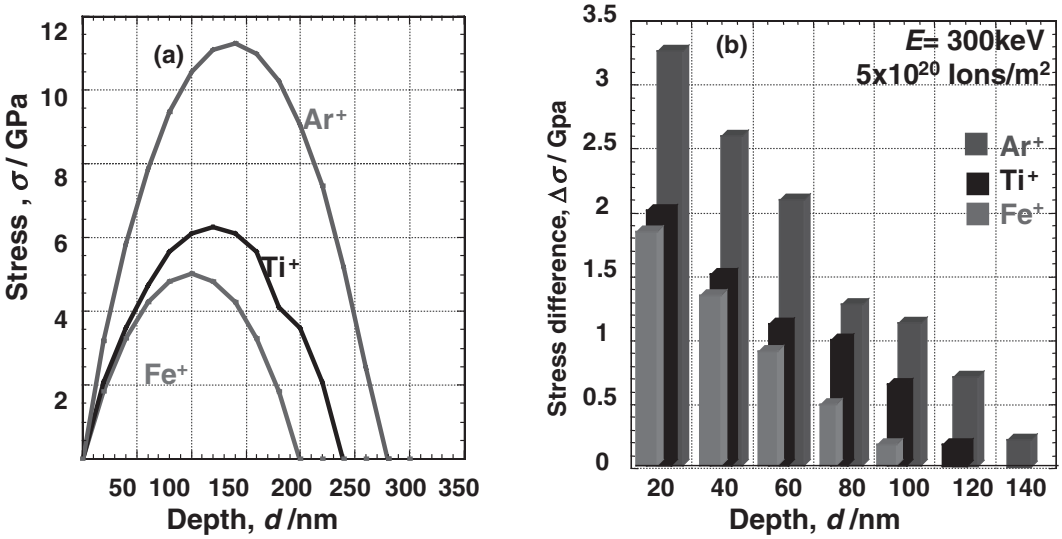

Fig. 7 Stress distribution profiles estimated from ion concentration implanted (a) and stress difference estimated from stress contribution profile in (b) at a given depth in the region with 20 nm width.

modulus 168 Gpa.[32] For instance, the estimated ε value at peak position of Ar^+ implanted specimen was about 0.069. The stress distribution profiles obtained from the estimation were similar to those of the concentration (Fig. 3(a)). Here, the contribution of damage defects was neglected because the amount of induced-defects were about one order less than that of implanted ions and furthermore most of defects would form defects clusters such as dislocations, so volume change cause by defects was assumed to be negligible small in present estimation even though radiation hardening would occur.

Figure 7(b) showed the stresses difference (corresponding to stress gradient) estimated from Fig. 7(a) with a interval of 20 nm depth from top surface up to the peak positions for each ions. It is recognized that the value of stress difference within 20 nm width was the highest at the top surface and then decreased with depth. As being observed in Fig. 6 the depth positions of initiation of the transformed phases were about 80 nm, 90 nm and 120 nm for Fe^+, Ti^+ and Ar^+, respectively. By considering the depths and the stress difference where the transformed phase was observed for each ion, it can be seen in Fig. 7(a) that the minimum stress difference to initiate the phase transformation was around 0.5 GPa at the depth of 80 nm for Fe^+ ion, therefore above this stress phase transformation would occur. This means that a critical stress difference corresponding to stress gradient or stress concentration applied to initiate the phase transformation may be about 0.5 GPa in 301 stainless steel due to the implantation of 5×10^{20} ions/m^2 at room temperature. This value is very close to stress for martensite nucleation discussed by Q. Wang *et al.*[33]

Thus it is assumed that the stress gradients caused by localized strain originated from implanted ion concentration would mainly contribute to initiation of martensite transformation under ion implantation, even though we have to consider strictly that damage defects could assist the initiation of transformation through the increasing of internal stress.

4. Summary

(1) Martensitic phase was induced with precipitate like distribution in austenite 301 stainless steel during Fe^+, Ti^+ and Ar^+ implantation, and the transformed phase was close to the Kurdjumov–Sachs relation of $[011]_\gamma$ // $[111]_\alpha$ and $(\bar{1}11)_\gamma$ // $(01\bar{1})_\alpha$.
(2) Martensitic phases were initiated close to specimen surface region, and the depth of the initiation depended on ion species and ion accelerating energy.
(3) The peak positions of the concentration of implanted ions and the defects calculated values by TRIM cod did not correspond to the position of initiation of transformed phases observed by cross-sectional observation.
(4) It was suggested that the stress effect due to volume change caused by concentration gradient of implanted ions acts as important driving force for the phase transformation.

REFERENCES

1) R. E. Fromson and R. Kossowsky: *Metastable Materials Formation by Ion Implantation*, ed. by S. T. Picraux and W. J. Choyke, (MRS, Massachusetts, 1982) pp. 355–362.
2) J. K. Hirvonnen: *Ion Implantation and Ion Beam processing of Materials*, ed. by G. K. Hubbler, *et al.* (MRS, Massachusetts, 1984) pp. 621–629.
3) F. G. Yost, E. L. Follstaedt, A. J. Knapp and S. T. Picraux: *Metastable Materials Formation by Ion Implantation*, ed. by S. T. Picraux and W. J. Choyke, (MRS, Massachusetts, 1982) pp. 261–268.
4) L. L. Singer and R. A. Jeffries: *Ion Implantation and Ion Beam processing of Materials*, ed. by G. K. Hubbler, *et al.* (MRS, Massachusetts, 1984) pp. 673–678.
5) L. Lau and P. Sioshanshi: *Ion Implantation and Ion Beam processing of Materials*.
6) I. L. Singer: Applic Surf. Sci. **18** (1984) 28–62.
7) P. J. Evans, J. Hyvarinen and M. Samanhadi: Surf. Coat. Technol. **71** (1995) 151–158.
8) S. Fayer, D. Treheux and P. Guiraldenq: Wea **122** (1988) 255–266.
9) A. A. Youssef, P. Budzynski, J. Filiks, B. Kamienska and D. Maczka: Vacuum **68** (2002) 131–137.

10) G. Bombara, M. Cavallini, G. Dearnaley, P. D. Goode and R. Fratesi: Surf. Technol. **18** (1983) 21–30.
11) F. J. Pez, M. P. Hierro, C. Gez, L. Martez and P. G. Viguri: Surf. Coat. Technol. **155** (2002) 250–259.
12) E. Johnson, T. Wohlenberg and W. A. Grant: Phase Transsit. **1** (1979) 21–34.
13) E. Johnson, U. Littmark and A. Johansen: Philos. Mag. **A45** (1982) 803–821.
14) N. Hayashi and I. Takahashi: Appl. Phys. Lett. **41** (1982) 1100–1101.
15) I. Hayashi, A. Sakamoto and T. Takahashi: J. Nucl. Mater. **128–129** (1984) 756–759.
16) S. Fayeulle, D. Trehuux and C. Esnouf: Nucl. Instrum. Meth. **B7–8** (1985) 171–176.
17) E. Johson, A. Johansen, L. Sarholt-Kristensen, H. Roy-Poulsen and A. Christiansen: Nucl. Instrum. Meth. **B7–8** (1985) 212–218.
18) N. Hayashi, E. Johson, A. Johansen, L. Sarholt-Kristensen and I. Sakamoto: Proc. Intre. Cof. on Martensitic Transformations (JIM, Nara-Japan, 1986) pp. 539–544.
19) E. Johnson, A. Johansen, L. Sarholt-Kristensen, L. Graaback, N. Hayashi and I. Sakamoto: Nucl. Instrum. **N19–20** (1987) 171–176.
20) E. Johnson, L. Graaback, A. Johansen, L. Sarholt-Kristensen, B. M. U. Scherzer, N. Hayashi and I. Sakamoto: Nucl. Instrum. Meth. **B39** (1989) 567–572.
21) N. Hayashi, I. Sakamoto and E. Hohson, (Proc. 12th Symp. ISIAT '89, Tokyo, 1989) pp. 495–500.
22) E. Johnson, A. Johansen, L. Sarholt-Kristensen, S. Steenstrup, Gerristsen, C. J. M. Denissen, H. Keetels, J. Politiek, N. Hayashi and I. Sakamoto: Nucl. Instrum. Meth. **B50** (1990) 119–126.
23) I. Sakamoto, N. Hayashi, B. Furubayashi and H. Tanoue: J. Appl. Phys. **68** (1990) 4508–4512.
24) I. Sakamoto, N. Hayashi, B. Furubayashi and Tanoue: J. Nuc. Mat. **179–181** (1991) 1053–1056.
25) G. Xie, M. Song, K. Mitsuishi and K. Furuya: J. Nucl. Mat. **281** (2000) 80–83.
26) N. Mottu, M. Vayer, P. Andreaz, T. H. Sauvge, G. Blondiaux and R. Erre: Surf. Coat. Techno. **151–152** (2002) 47–50.
27) S. Raud, H. Garem, A. Naudon, P. J. P. Villain and P. Moine: Mat. Sci. Eng. **A115** (1989) 245–251.
28) D. Gustiono, N. Sakaguchi, T. Shibayama, H. Kihoshita and H. Takahashi, (The Fourth Pacific Rim Inter. Conf. on Advanced Materials and Processing (PRICM4), 2001, JIM) pp. 1497–1499.
29) D. Gustiono, N. Sakaguchi, T. Shibayama, H. Kinoshita and H. Takahashi: J. Electron Microscopy **52** (2003) 559–453.
30) D. Gustiono, N. Sakaguchi, T. Shibayama, H. Kinoshita and H. Takahashi: Mat. Trans. **45** (2004) 65–68.
31) G. Kurdjumov and G. Sachs: Z. F. Phys. **64** (1930) 325–343.
32) *Chronological Scientific Tables*, ed. National Astronomical Observatory, (Maruzen Co. Ltd).
33) Q. Wang, H. Ogiso, S. Nakano, J. Akedo and H. Ishikawa: *Nuclear Instruments and Methods in Physics Research Section B: Beam Interactions with Materials and Atoms, Volume 206*, May 2003, pp. 118–122.